遐期汇集

1978年—1996年

第一册

复旦大学环境科学研究所

近期汇集

1978年－1996年

第一册

复旦大学环境科学研究所

目　录

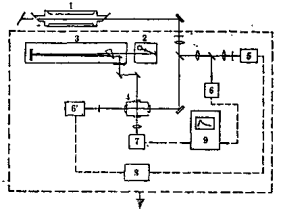

1—TEA CO_2 激光器；2—全反镜；3—半反镜；4—样品池；5—光电探头；6—热电探头前置放大器；7—光电管前置放大器；8—记忆示波器；9—示波器。

图 1 UF_6 振动受激态的紫外吸收测定实验装置

结 果 和 讨 论

若将单一的 SF_6 或 UF_6 气体分别充入样品池，经脉冲 CO_2 激光(400 mJ/脉冲)辐照，都未发现在上述的紫外波长范围内有吸收信号的变化．再将分压各为 2.0 Torr SF_6 和 UF_6 的混合气体，用脉冲 CO_2 激光辐照，在示波器上也未见有信号出现．但是，将上述混合气体经 CO_2 脉冲激光和紫外探测光同时辐照，即出现明显的紫外吸收信号的变化．图 2 为波长在 240 nm 时测得的结果．可见，该信号来自振动激发态 UF_6 紫外吸收截面的变化．此外，该样品池内的混合气体，在上述实验条件下经红外激光脉冲辐照数百次，都未发现其中 UF_6 的分压有变化，表明没有 UF_6 解离．

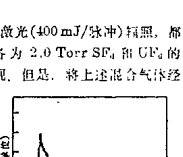

图 2 UF^* 在 240 nm 时紫外吸收信号变化
(2.0 Torr SF_6 + 2.0 Torr UF_6)

UF_6 紫外吸光度的变化 假设在室温下 UF_6 对一定波长的紫外光的吸光度为 A_0，经红外激光辐照和 SF_6 光敏激发后 UF_6 的吸光度为 A^*．按 Beer 定律可写出：

$$A_0 = n_0\sigma_0 l + \sum_i n_i\sigma_i l \qquad A^* = n_0^*\sigma_0 l + \sum_i n_i^*\sigma_i l$$

其中 n_0 和 n_0^* 是 UF_6 分别在红外激光辐照前后处于振动基态的布居数，n_i 和 n_i^* 分别是它们处于各个振动激发态的布居数，σ_0 和 σ_i 分别是分子处于基态和第 i 个振动激发态时对某紫外波长光的吸收截面，l 是紫外光束与红外激光束相交处的光程．按上述关系可以认为激光辐照前后 UF_6 分子处于基态的布居数变化等于各振动激发态上布居数变化的加和，即

$$n_0 - n_0^* = \sum_i (n_i^* - n_i).$$

由此可得实验测定的紫外吸光度的瞬时变化：

$$\Delta A = A_0 - A^* = l\sum_i (n_i^* - n_i)(\sigma_0 - \sigma_i). \qquad (1)$$

由上式可知，在波长一定时 $\sum_i (\sigma_0 - \sigma_i)$ 值对 ΔA 的贡献是不变的，l 又是常数，则 ΔA 正比于 $\sum_i (n_i^* - n_i)$，而后者与激光能量，SF_6 和 UF_6 的分压都有关系．因此必须分别固定上述因素对 UF_6 紫外吸收瞬时变化的影响．

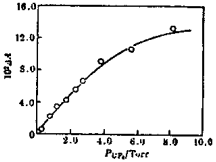

图5 UF_6分压对 ΔA 的影响

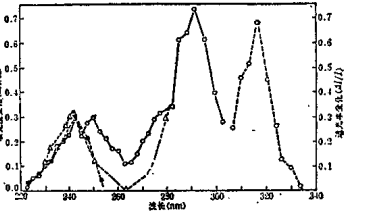

图6 振动受激 UF_6 分子吸收变化与波长的关系

○—3.0 Torr+2.0 Torr UF_6 在室温下经 10.6 μm CO_2 激光激发

△—超声射流 UF_6 经 16 μm 激光直接激发[3]

●—超声射流 SF_6+UF_6 经 10.6 μm CO_2 激光激发

得的 $\Delta A/A_0$ 值随波长变化的趋势与 Kim 等[2] 的实验结果基本上是一致的. 但是本文测得的紫外瞬时吸收变化在 240, 243 和 290 nm 处分别出现三个峰, 而 Kim 等只在 240 nm 附近出现一个高峰. 这可能是因在超声射流冷却条件下的 UF_6 分子很少被热激发, 这样振动激发态上分子的布居要比本文在室温和压力较高的条件下简单得多. 我们在前文[4] 中测得在波长大于 240 nm 处出现几种不同的振动激发态 UF_6 分子也可作为旁证.

在波长为 300—340 nm 处, 由于 UF_6 的吸收截面很小, 以 $\Delta A/A_0$ 表示振动受激 UF_6 分子的吸光度变化产生的误差很大. 为此, 我们改用 $\Delta I/I_0$, 即红外激光辐照混合气体的前后样品池透过紫外光强的相对变化值表示. 从图 6 的右边部分可以看出, 在 313 nm 处呈现明显的高峰. 在此波长附近振动激发态 UF_6 分子的吸收截面约比基态时提高了 10 倍以上. 这样, 可以考虑通过红外-紫外双激发使 UF_6 分子选择性解离, 有可能获得同位素分离的效果.

六氟化铀紫外吸收光谱的归属一直是十分困难而又有兴趣的课题[5]. 一般在 220—340 nm 范围内是属于 UF_6 更高电子受激态的 B–$\tilde{X}$ 带, 但是相应于 B–$\tilde{X}$ 带的振动受激 UF_6 分子的紫外吸收光谱要更为复杂, Kim 等[2] 将在 240 nm 处的吸收峰归结为相应的基态 UF_6 分子在 220 nm 处吸收峰的红移, 该 16 μm 红外光子能量计算约为 8 个光子. 至于图 6 中在 248, 290, 和 313 nm 处的吸收峰, 较难由红移来解释, 而这些处于高振动激发态 UF_6 分子的性质有待于进一步研究.

本文系中国科学院科学基金资助的课题.

参 考 文 献

[1] Kim, K. C.; Freund, S.; Sander, R. K.; Slith. D. F.; Person, W. B., *J. Chem. Phys.*, 1983, *79*, 33.
[2] Kim, K. C.; Freund, S. M.; Sorem, M. S.; Smith, D. F., *J. Chem. Phys.*, 1985, *83*, 4384.
[3] 侯惠奇, 何志强, 张启荣, 化学学报, 1985, *43*, 24.
[4] 蔡中辉, 侯惠奇, 蔡启荣, 物理化学学报, 1987, *3*, 197.
[5] Angelie, C.; Cauchetier M.; Paris, J., *Chem. Phys.*, 1982, *66*, 129.
[6] McDiarmid, *R., J. Chem. Phys.*, 1976, *65*, 168.

The Changes in UV Absorbance of the Vibrationally Excited UF_6 Molecules

Hou Hui-Qi　Cai Zhong-Hou　Qin Qi-Zong*

(Laser Chemistry Laboratory, Fudan University, Shanghai)

Abstract

The transient changes in UV absorbance of the vibrationally excited UF_6 molecules in the UV region of 220—330 nm have been investigated. The UF_6 molecules are excited from pulsed CO_2 laser pumped SF_6 by a V–V energy transfer process. Under static condition, the influences of CO_2 laser fluence, SF_6 and UF_6 partial pressure upon the UV absorption changes have been measured. For a 2.0 Torr SF_6 and 2.0 Torr UF_6 mixture and at laser pulsed energy of 160±10 mJ, the UV absorption spectrum of vibrationally excited UF_6 molecules shows existence of four absorption peaks at 240, 248, 290 and 313 nm, respectively. It may be related to the UV absorption of several higher vibrationally excited UF_6 molecules.

Observation of competing arsenic removal channels in the Cl_2+GaAs reaction

Hui-qi Hou,[a] Zhuangjian Zhang,[b] Shanhua Chen,[c] Chaochin Su, Weiring Yan, and Matt Vernon[d]
Department of Chemistry, Columbia University, New York, New York 10027

(Received 6 April 1989; accepted for publication 8 June 1989)

A molecular beam study of the Cl_2 + GaAs(*s*) reaction has been performed for surface temperatures in the range of 300–550 K. The gas phase neutral reaction products are identified by mass spectroscopy using electron bombardment ionization. Detailed analysis of the surface temperature dependence of the mass spectrum of the observed reaction products indicates that only three neutral reaction products are formed in this temperature range: $GaCl_3$, $AsCl_3$, and As_4. At low (high) surface temperatures, only $AsCl_3$ (As_4) is observed. The ratio of the etching rates of Ga and As is independent of the surface temperature and within the range expected for stoichiometric etching. The change in the mode of As removal with surface temperature for the incident Cl_2 flux implies that surface diffusion is important at surface temperatures above 400 K.

The etching reaction of Cl_2 and/or Cl with GaAs(*s*) is an important process in semiconductor processing. In order to control the physical and chemical properties of the surface profile resulting from the chlorine etching reaction, knowledge of the reaction mechanism is required. In the studies of the etching reaction to date, the separate and combined effects of optical radiation,[1] doping,[2] charged particles,[3] and other chemically reactive species have been investigated.[4] Although much is known empirically about the etch rates and their dependence on process conditions (substrate temperature, plasma power, flow rates, etc.), comparatively little is known about the underlying surface chemical processes responsible for etching. In this letter we report recent results of a molecular beam scattering experiment of the reaction Cl_2 + GaAs where all major Ga and As etching products have been identified for surface temperatures (T_s) from 300 to 550 K.

The reactive scattering experiments were performed in a crossed molecular beam apparatus which has been previously described.[5] The supersonic Cl_2 molecular beam is formed by expanding a mixture of 5% Cl_2/95% He though a 0.005-in.-diam graphite nozzle. The graphite nozzle can be resistively heated to ~1500 K to thermally dissociate Cl_2 to make Cl atoms.[6] A graphite skimmer allows the 3° on-axis portion of the molecular beam to pass into a second vacuum chamber where the GaAs surface is located. The GaAs sample is attached to a copper block by a high-temperature cement. (T_s) is measured by a chromel-alumel thermocouple bonded to the surface by the high-temperature cement. The actual surface temperature in the etched region may deviate from the thermocouple reading as a result of a different surface emissivity for the chlorinated surface and the exothermicity of the etching reaction. The GaAs sample was etched with a bromine/methanol solution immediately, prior to installation in the vacuum chamber to minimize the thickness of the surface oxide.

The neutral reaction products of the Cl_2/GaAs reaction are detected by a rotating mass spectrometer utilizing an electron bombardment ionizer (located ~21 cm from the surface) housed in a triply differentially pumped, liquid-nitrogen-cooled vacuum chamber, a rf quadrupole mass filter, and a Daly ion detector. The GaAs surface assembly can be translated to intercept the molecular beam or removed so that the velocity distribution and intensity of the molecular beam can be measured by time-of-flight techniques. For the experiments reported here, the Cl_2 molecules are incident at a 65° angle to the surface normal with ~0.15 eV translational energy normal to the surface. The mass spectrometer samples the products desorbed at the surface normal. The angular and velocity distributions of the Ga- and As-containing products measured at other scattering angles show that the product mass distribution measured at the surface normal is representative of the integrated product mass distribution.

The procedure for determining the reaction products was as follows. At the start of an experiment, the graphite nozzle was heated to make Cl atoms to clean the surface of oxides or contaminants which have accumulated on the surface. We estimate that ~1000 monolayers of GaAs are etched during the surface cleaning procedure. After the nozzle temperature returned to room temperature, the mass spectrometer was then scanned by a computer, accumulating data for 50 ms every 0.2 amu. T_s was then changed and the mass range scanned again. So long as the surface is first cleaned with the Cl atom beam, the absolute count rates are reproducible at all T_s and independent of the previous value of T_s. At the highest T_s of this study, the approximate etch rate determined from the observed signal after correcting for the ionization efficiency and solid angle sampled by the detector is 4 ML/s. The pressure in the vacuum chamber housing the surface is $\sim 1\times 10^{-6}$ Torr when the molecular beam is operating. We detect no significant mass signals that arise from contaminants and conclude from the reproducibility of

[a] Permanent address: Department of Nuclear Science, Fudan University, Shanghai, People's Republic of China.
[b] Permanent address: Department of Physics, Fudan University, Shanghai, People's Republic of China.
[c] Department of Physics, The Second Institute of Education of Shanghai, People's Republic of China.
[d] Person to whom correspondence should be addressed.

 0003-6951/89/340801-03$01.00

the experiments that the vacuum is sufficient for the purpose of determining the major etching reaction products.

Figure 1 shows two typical mass spectra obtained at T_s of 349 and 548 K. The large number of mass peaks observed is a result of the isotope distribution of ^{69}Ga, ^{71}Ga, ^{35}Cl, and ^{37}Cl. The mass resolution of the quadrupole filter is adjusted to give a ~75% dip between two masses of equal intensity separated by two mass units. Using the known isotopic abundances, it is possible to extract the separate contributions when more than one etch product is detected at the same mass. For example, $^{75}As^{35}Cl_2^+$ and $^{71}Ga^{37}Cl_2^+$ contribute to the detected signal at mass 145. The signals observed at $As^+(m/e = 75)$ and $Ga^+(m/e = 69,71)$ are small compared to the signals shown in Fig. 1 and are not shown because of the large Cl_2^+ $(m/e = 70,72,74)$ signal from scattered Cl_2.

Figures 2 and 3 show the T_s dependence of the dominant mass peaks after correcting for the isotopic distribution. From the data shown in Figs. 2 and 3 it can be seen that the ions can be divided into three groups according to their T_s dependence: ($GaCl^+$, $GaCl_2^+$, and $GaCl_3^+$), ($AsCl^+$, $AsCl_2^+$, $AsCl_3^+$), and (As_2^+, As_3^+, and As_4^+). Within a particular group, the T_s dependence of the different ions is identical within experimental error. This indicates that there are three major neutral reaction products which ionize to give the distribution of parent and daughter ions observed: $GaCl_3$, $AsCl_3$, and As_4. We have checked for additional signals at all possible combinations of Ga, As, and Cl to the ~350 upper mass limit of our quadrupole mass filter without observing significant signals at any other masses.

The major difference between the current and prior investigations[7] of the Cl_2 + GaAs reaction is the observation that there are two distinct mechanisms for the removal of As. At low T_s, As is removed as $AsCl_3$, while at higher T_s it is removed only as As_4. To our knowledge, this is the first time that As_4 products have been observed in the Cl_2 + GaAs etching reaction. In the chloride vapor transport growth of GaAs from Ga/HCl and arsine,[8] the arsine is thermally cracked to As_4 and As_2. The temperatures used typically exceed 700 K and therefore are significantly hotter than the experimental conditions of this study.

Although we expect that in the steady state, Ga and As are removed at equal rates, it is difficult to show positively that, in fact, the rates are equal in a given experimental apparatus. It could be possible for Ga or As to segregate on the surface as observed in the evaporation of GaAs.[9] In our experiment, if the mass dependence of the transmission of the

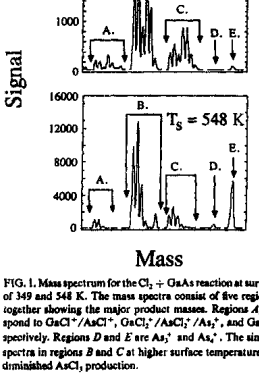

FIG. 1. Mass spectrum for the Cl_2 + GaAs reaction at surface temperatures of 349 and 548 K. The mass spectra consist of five regions, *A–E*, spliced together showing the major product masses. Regions *A*, *B*, and *C* correspond to $GaCl^+/AsCl^+$, $GaCl_2^+/AsCl_2^+/As_2^+$, and $GaCl_3^+/AsCl_3^+$, respectively. Regions *D* and *E* are As_3^+ and As_4^+. The simplification of the spectra in regions *B* and *C* at higher surface temperature is a result of the diminished $AsCl_3$ production.

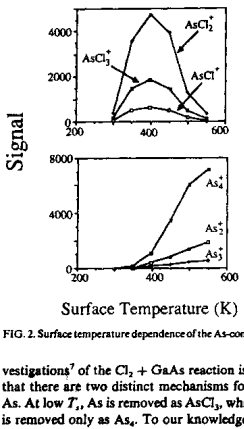

FIG. 2. Surface temperature dependence of the As-containing product ions.

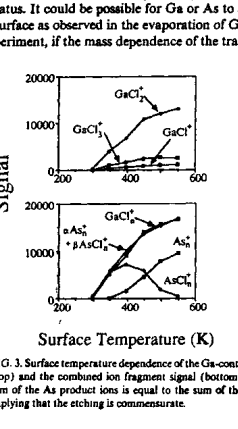

FIG. 3. Surface temperature dependence of the Ga-containing product ions (top) and the combined ion fragment signal (bottom) showing that the sum of the As product ions is equal to the sum of the detected Ga ions implying that the etching is commensurate.

mass spectrometer is known, then to determine the relative intensities of different neutral products requires only knowledge of the relative total ionization cross sections of the three reaction products, because we detect all of the ion fragments of each reaction product. Unfortunately, experimental determination of the total ionization cross sections is difficult and they have not been measured for all three reaction products.

To show then that the data are indeed consistent with equal As and Ga etching rates, we search for constant, T_s-independent, multiplicative factors α and β for the As_4 and $AsCl_3$ signals such that

$$GaCl_3 = \alpha * As_4 + \beta * AsCl_3. \quad (1)$$

The empirical fit resulting from the best values, $\alpha = 1$ and $\beta = 1.7$, is shown in Fig. 3. Within experimental error, the mass spectroscopy results are consistent with a T_s-independent ratio of the etching rates for As and Ga.

We can independently estimate the values of α and β to show that they are within the range that we expect for the stoichiometric reaction. To first order, the molecular ionization cross sections are proportional to the square root of the molecular polarizabilities.[10] The molecular polarizability is approximated by the sum of the atomic polarizabilities.[11] Second, the ionization efficiency is inversely proportional to the velocities of the neutral products. If thermalized, the velocities are proportional to the inverse square root of the product mass. The velocity dependence and ionization probability can be combined into a single correction factor to convert the number of detected ions per second to desorbed flux. These flux correction factors predict $\alpha \sim 1$ (because at low T_s only $AsCl_3$ is observed and the trichlorides have similar masses and ionization cross sections) and $\beta \sim 4/2 = 2$ (because at high T_s only As_4 is present, removes 4 As atoms and is ionized twice as efficiently as the trichlorides). The experimentally optimized values of the relative ionization cross sections ($\alpha = 1$, $\beta = 1.7$) are close to the predicted values based on this simple model of the ionization cross sections.

Thermodynamic calculations of the Ga/As/Cl system[8] indicate that at the T_s of this study, $GaCl_3$ and As_4 should be the major products. Observation of $AsCl_3$ indicates a kinetic restriction. One kinetic limitation could be that at low T_s, the effective Cl^7 mobility is low. If there is no diffusion of any species at low T_s and Cl_2 can react readily with both Cl-deficient As and Ga sites on the surface, then only the $GaCl_3$ and $AsCl_3$ products would be formed as observed. For the thermodynamically favored products ($GaCl_3$ and As_4) to be formed if Cl-deficient Ga and As are both reactive, any Cl which has reacted with As must be mobile and able to encounter and exchange Cl with an unsaturated Ga site before desorbing. From our experiments, we could conclude that for $T_s > 350$ K, any $AsCl_x$ initially formed when Cl_2 collides with a reactive As site begins to transfer its Cl atoms to Ga. The excess As is removed as As_4 at these T_s because it is a volatile As species, reacts without dissociation with vacant Ga sites,[12] and is thermodynamically favored. [Note that we are below the T_s for evaporation of As_4 (Ref. 12) or As_2 (Ref. 9) from the solid.]

A second alternative explanation could be that at high T_s there is insufficient Cl_2 flux to fully chlorinate all of the surface As compared to the rate of formation and desorption of As_x. To illustrate tha differences in the two explanations, assume that Cl surface diffusion is possible at all T_s of our experiments. If at low T_s there is sufficient Cl_2 flux to saturate both the Ga and As sites, then the desorption rate of the slowest etch product must be less than some value which is determined by the specific Cl_2 flux. As T_s increases, the rate of the slowest desorption step also increases so that eventually tha fixed Cl_2 flux is insufficient to fully chlorinate all As and Ga sites. At this point, if the Cl bound to As can diffuse to and bond with a Cl-deficient Ga site, the etching reaction rate can continue to increase because Ga can only be removed as a chloride from the surface while As can desorb as As_x. If tha rate of As_x formation and vaporization is faster than $GaCl_3$ desorption and the As bound Cl is mobile, then a high etching rate of GaAs can be maintained for the limited Cl_2 flux.

In conclusion, a molecular beam scattering experiment of the Cl_2 + GaAs reaction has been performed which has identified the major reaction products. At all T_s studied, $GaCl_3$ is the only Ga-containing product while $AsCl_3$ and As_4 competa for the removal of As. $AsCl_3$ is the only As-containing product formed at low T_s, while at higher T_s, only As_4 is formed. We heve considered two explanations for the change in the mechanism of removing As. One postulates tha thermally activated mobility of Cl initially bound to As as the limiting kinetic process, while the second ascribes the change to the limited Cl_2 flux. Future experiments which measure the product velocity distributions when the incident molecular beam is modulated and the Cl_2 flux dependence of the competing As products will provide experimental data on the kinetics of the etching reaction to distinguish between the two models.

This work was supported by a Presidential Investigator Award from the National Science Foundation (CHE-85-52744) and a matching grant from the Ford Motor Company. MFV thanks Brian Bent for many discussions on surface reactions.

[1]Q. Z. Qin, Y. L. Li, Z. K. Jin, Z. J. Zhang, Y. Y. Yang, W. J. Jia, and Q. K. Zhang, Surf. Sci. 207, 142 (1988).
[2]C. I. H. Ashby, Appl. Phys. Lett. 48, 892 (1984).
[3]W. L. O'Brien, C. M. Paulsen-Boaz, T. N. Rhodin, and L. C. Rathbun, J. Appl. Phys. 64, 6523 (1988).
[4]J. A. Skidmore, L. A. Coldren, E. L. Hu, J. L. Merz, and K. Asakawa, J. Vac. Sci. Technol. B 6, 1885 (1988).
[5]U. Ray, S. L. Brandow, G. Bandukwalla, B. K. Venkataraman, Z. Zhang, and Matt Vernon, J. Chem. Phys. 89, 4092 (1988).
[6]J. J. Valentini, M. J. Coggiola, and Y. T. Lee, Rev. Sci. Instrum. 48, 58 (1977).
[7]M. Balooch, D. R. Olander, and W. J. Siekhaus, J. Vac. Sci. Technol. B 4, 794 (1986).
[8]Christian Chatillon and Claude Bernard, J. Cryst. Growth 71, 433 (1985).
[9]J. R. Arthur, Surf. Sci. 43, 449 (1974).
[10]R. E. Center and A. J. Mandl, J. Chem. Phys. 57, 4104 (1972).
[11]T. M. Miller and B. Bederson, Adv. Atom. Molec. Phys. 13, 1 (1977).
[12]C. T. Foxon and B. A. Joyce, Surf. Sci. 50, 434 (1975).

G.Marx, A.Bestanpouri, R.Droste, W.Schönemann, D.Wegen and Hou Hui-qi
Institute for Inorg. and Analyt.Chem.
Dept.of Radiochemistry, FU Berlin (F.R.G.) and
Fudan University, Nuclear Sc.Dept. (Shanghai/China)

RADIOCHEMICAL INVESTIGATIONS ON CORROSION OF VALVE METALS AND STAINLESS STEEL UNDER THE INFLUENCE OF PLUTONIUM

In presence of Plutonium under the practical conditions of the PUREX process the corrosion behaviour of valve elements (Hf, Ti,Zr,Ta, Nb) and stainless steel was investigated by use of impedance measurements in addition to radiochemical and electrochemical methods, based upon a new technique of combined applications of neutron activation analysis and normal electrochemical procedures. This new radioisotopic method has the advantage to be able to determine simultaneously the amount of material dissolved due to corrosion and also that special quantity being used for forming the oxide layer of the valve metals. In addition the impedance measurements also performed simultaneously give informations about the oxide layer, its physical structure and characteristics being changed by the amount of plutonium, incorporated.

Last but not least the radioisotope method applied to the investigations on stainless steel makes practical anodic and cathodic currents be calculated from the corrosion rate of the various components of the alloys, labelled by NAA, which for the first time makes informations about partial corrosion be obtained continuously. The influence of Fission products and of materials dissolved by corrosion on the corrosion potentials of stainless steel, were investigated systematically at various temperatures and at a variety of HNO_3 concentrations. In addition the corrosion behaviour of stainless steel in presence of plutonium has been intensively studied, including investigations of the surface by use of various methods.

- 252 -

A crossed laser-molecular beam study of the one and two photon dissociation dynamics of ferrocene at 193 and 248 nm

Urmi Ray,[a] Hui Qi Hou,[b] Zhvangjian Zhang,[c] and Wolfgang Schwarz,[d] and Matt Vernon

Department of Chemistry, Columbia University, New York, New York 10027

(Received 3 October 1988; 15 December 1988)

A crossed laser-molecular beam study of the one and two photon dissociation mechanism of bis (cyclopentadienyl) iron (ferrocene, $FeCp_2$) has been performed at 193 and 248 nm. By combining electron bombardment mass spectroscopy with time-of-flight (TOF) measurements, the photodissociation mechanism at 193 nm is shown to have two distinct mechanisms. (1) $FeCp_2 + h\nu \rightarrow FeCp^* + Cp$; (2) $FeCp + 2h\nu \rightarrow FeCp^{\#} + Cp$, $FeCp^{\#} \rightarrow Fe + Cp$. For the first mechanism, which accounts for less than 5% of the photodissociation events, the $FeCp^*$ velocity distribution is quantitatively consistent with a statistical dissociation producing FeCp in an excited, ligand field electronic state. The velocity distributions of the Cp and Fe fragments produced by the second mechanism ($FeCp^{\#}$ is an unstable intermediate) are also in excellent agreement with microcanonical calculations for both Cp elimination steps using the known metal–ligand bond energies of ferrocene. For the second mechanism, dissociation occurs on the lowest potential energy surface for each Cp elimination. Although one photon is energetically sufficient to remove one Cp ligand from ferrocene, RRKM calculations of the lifetime indicate that Cp elimination is extremely slow for dissociation along the ground electronic state potential energy surface. Hence, after internal conversion to the ground electronic state, the large photon absorption cross section (~ 4 Å^2) for the experimental irradiation conditions allows additional photons to be absorbed until the dissociation rate exceeds the up pumping rate. The large photon energy causes the dissociation rate to increase by many orders of magnitude for each additional photon absorbed. Consequently, there is strong selectivity for the total number of photons absorbed. Both mechanisms, occurring on two different electronic potential energy surfaces, suggest that dissociation induced by excitation of the ligand-to-metal charge transfer states accessed at 193 nm can be quantitatively described as a statistical, unimolecular decomposition. At 248 nm, the measured product velocity distributions are qualitatively consistent with the mechanism deduced from the 193 nm results, but the energy available for translation at this wavelength is too small to extract quantitative product translational energy distributions which are required to independently test the applicability of the statistical dissociation model.

INTRODUCTION

The electronic structure of metal–sandwich compounds, especially ferrocene, has been the subject of many theoretical and experimental investigations.[1–7] Of particular interest is whether the η^5 bonding exhibits unusual photochemical behavior. The electronic absorption spectrum for ferrocene is well known and the features in the spectrum can be assigned to specific excited state electronic configurations.[4] The strongest band is centred at 50 000 cm^{-1} (molar absorption coefficient $\epsilon = 51\,000$ M^{-1} cm^{-1}) and is attributed to the dipole allowed, $^1A_{1g} \rightarrow {}^1A_{2u}$ ligand-to-metal charge transfer (L→MCT) transition.[4] The transition, polarized along the Cp–Fe–Cp axis, involves promoting an electron from the $1e_{1u}$ to the $2e_{1g}$ orbital (see Fig. 2). It is proposed that the absorptions at 41 000 and 42 800 cm^{-1} are dipole allowed, metal-to-ligand charge transfer bands (M→*LCT*) involving the $1e_{2g} \rightarrow 1e_{2u}$ orbital excitation. The lower energy (20 000–30 000 cm^{-1}) bands are much weaker and can be assigned to spin-allowed, electric dipole forbidden, *d–d* ($1e_{2g}$ or $2a_{1g} \rightarrow 2e_{1g}$), ligand field (LF) transitions. There is also at least one experimentally identifiable band at $\sim 18\,600$ cm^{-1}, which is assigned to a spin-forbidden, LF transition.

Although the relative ordering of the valence orbitals appears correctly given by converged Hartree–Fock calculations, other properties are not as accurate. On the basis of SCF-$X\alpha$ calculations,[5] the assignments of the observed optical spectra are very different than those given by CI assignments.[7] Theoretical calculations of the metal-to-ring bond distance, by *ab initio* MO-SCF calculations[6] of better than triple-zeta quality, exceed the experimental value by 15%. Inclusion of configuration interaction[7] shows that the Hartree–Fock wave function is too ionic. Inspection of the wave functions involved in the CI expansion indicate that as the Fe–Cp distance changes in the bonding region, the largest electronic effect does not involve charge transfer between the metal and ligands, but rather a rearrangement of the relative contributions of the metal atom e_{1g}, e_{2g}, and a_{1g} *d*-orbitals.

[a] Present address, AT&T Bell Laboratories, Murray Hill, NJ 07974

[b] Department of Nuclear Science, Fudan University, Shanghai, The People's Republic of China

[c] Department of Physics, Fudan University, Shanghai, The People's Republic of China.

[d] Department of Physics, Columbia University, New York, New York 10027.

 0021-9606/89/084248-10$02.10

A number of multiphoton dissociation (MPD)–multiphoton ionization (MPI) studies of ferrocene have been reported. Two early MPD/MPI studies,[8,9] which measured total ion current, observed a broad, structureless continuum with superimposed resonances of 50 times greater intensity throughout the wavelength range 3750–4500 Å. The continuum was assigned to molecular ion fragments while the resonant peaks could all be assigned to one or two photon resonances of Fe atoms. This interpretation implied that two competing processes were occurring—ferrocene could absorb several photons exciting successively higher energy electronic states until ionization occurred, or the absorption of photons could result in Cp ring eliminations eventually producing atomic iron which then resonantly ionizes by MPI. A third study,[10] which mass resolved the positive ion fragments, showed that only Fe^+ ions were produced in the continuum background region from 3750–4200 Å. Since two photon ionization of ferrocene is not energetically possible at these wavelengths, it was concluded that Cp elimination producing FeCp, followed by nonresonant production of Fe^+ via the FeCp intermediate, was occurring.

More recently, Nagano, Achiba, and Kimura[11] have measured the MPD/MPI spectrum of ferrocene in the 366.5–370 nm wavelength region by monitoring the positive ion current and the photoelectron kinetic energy distribution. From their experimental results they propose a mechanism in which electronic to vibrational energy conversion occurs on a faster time scale than the Fe–Cp bond dissociations. Since the authors do not observe any molecular ions in the 370–366 nm wavelength range, they postulate a multiphoton dissociation mechanism involving stepwise Cp elimination; although they cannot unequivocally rule out a concerted elimination of both Cp ligands from their experimental results.

Liou, Engelking, Ono, and Moseley[12] and Liou, Ono, Engelking, and Moseley[13] have performed several MPD experiments on ferrocene to determine if there is a wavelength dependence of the dissociation pathway which produces Fe atoms. In one set of experiments, a single laser frequency of 447.65 nm was used to both dissociate ferrocene and probe the velocity distribution of the Fe atoms. At this wavelength, a minimum of three photons are energetically required to produce Fe atoms. If three photons are absorbed, the maximum energy available after breaking both Fe–Cp bonds is 46 kcal/mol. The velocity of the Fe atoms was measured by the Doppler line profile of a three photon MPI process. The Doppler profile indicates an averge iron atom translational energy of ~16 kcal/mol. Since the three fragments have nearly equal masses, the authors concluded that nearly all of the available energy appears as photofragment translation. To channel such a large fraction of the available energy into translation, it was further argued that the excited state potential energy surface was repulsive. In analogy with metal alkyl photodissociation,[14] the authors favored a two step ejection of the Cp ligands [Eq. (2)] rather than a concerted elimination [Eq. (1)].

In a separate series of experiments, a second laser frequency of 351 or 248 nm was used in addition to the ~440 nm frequency required for MPI detection of the Fe atoms. With 351 nm radiation, there was no change in either the intensity or state distribution of the Fe atoms probed by MPI. Since the product of the laser intensity and the ferrocene absorption coefficient at 351 nm is approximately the same as used in the single color ~440 nm experiments, the authors conclude that ferrocene must be absorbing the 351 nm radiation. To explain the absence of any apparent effect by the 351 nm radiation, the energy deposited by the 351 nm photons is assumed to be rapidly converted to vibrational motions of the ground electronic state in such a way as to be ineffectual in either breaking a Fe–Cp bond or in producing a different electronic state distribution of the Fe atoms probed by the 440 nm radiation. On the other hand, 248 nm radiation produces Fe atoms in numerous excited electronic states unobserved with only 440 nm radiation. This contrasting wavelength dependence was explained by the absence of a repulsive excited electronic surface accessible at 351 nm while at 248 nm, two photons provide enough energy for dissociation to occur on an excited, repulsive surface.

The consensus of the MPD/MPI studies is that both Cp ligands are lost prior to ionization, however, the detailed mechanism of photon absorption and subsequent ligand loss has not been unequivocally established. In particular for multiphoton dissociation, three qualitatively different photodissociation pathways can be envisioned.

(i) Photon absorption followed by concerted, multiple ligand loss

$$FeCp_2 + nh\nu \rightarrow Fe + 2Cp. \quad (1)$$

(ii) Photon absorption followed by sequential ligand loss via an unstable intermediate

$$FeCp_2 + nh\nu \rightarrow FeCp + Cp \rightarrow Fe + 2Cp. \quad (2)$$

(iii) A sequence of photon absorption, ligand elimination steps

$$FeCp_2 + nh\nu \rightarrow FeCp + Cp, \quad (3)$$

$$FeCp + mh\nu \rightarrow Fe + Cp. \quad (4)$$

The number of photons required and the pathway will depend on the photon energy, intensity, and the molecule specific details of the photodissociation process.

Analysis of thermochemical data[15] was used to derive that 142 kcal/mol is required to break both metal–ligand bonds. Low pressure pyrolysis experiments performed by Lewis and Smith[16] have directly determined the first FeCp–Cp bond energy to be 91 ± 3 kcal/mol, which sets the second Fe–Cp bond energy value at 51 kcal/mol using the thermochemical value from Ref. 15. J. P. Puttemans, G. Smith, and D. Golden[24] have noted that the metal–sandwich bond energies given in Ref. 15 used a value for the Cp heat of formation which is probably too low by 8 kcal/mol. If a more reasonable value of 58 kcal/mol for the Cp heat of formation is used, then the second bond dissociation energy of ferrocene would be 67 kcal/mol. With an accurate knowledge of both metal–ligand bond energies, the minimum number of photons required in the experiments of Liou *et al.* can be determined. For 448 and 351 nm radiation, a minimum of two photons of either color is required to break the first Fe–Cp bond. For 448 nm radiation alone, at least three photons

are required to break both Fe–Cp bonds, while a combination of two 448 nm and one 351 nm photon or two 351 nm photons meets the energy requirements for breaking both Fe–Cp bonds. A single 248 nm photon can break the first Fe–Cp bond, while a combination of one 448 nm and one 248 nm photon or two 248 nm photons are necessary to break both Fe–Cp bonds. Of course, in the sequential bond breaking models, if a significant amount of energy is carried away in translational motion or as vibrational excitation of the first Cp fragment, additional photons might be required to produce atomic Fe. Figure 1 shows the relationship between the metal–ligand bond dissociation energies and the photon wavelengths for the present and previous experimental studies.

From the above discussion it is clear that further work is necessary to understand the primary photodissociation dynamics of ferrocene. Figures 2 and 3 show simple, molecular orbital correlation diagrams for breaking the first and second Fe–Cp bonds.[17] The allowed electronic transition accessible at 193 nm in ferrocene correlates with the ground, $^3E_1$ state of FeCp. Absorption of a second 193 nm photon by FeCp would, by analogy, correspond to exciting an electron from the $1e_1$ to the $2e_1$ orbital in the C_s point group (the transition $^2E_1 \rightarrow {}^2A$ is allowed), which, after the loss of a Cp ligand, correlates to the ground state of Fe $[(1e_2)^4(2a_1)^2(2e_1)^2]$. Hence, the sequential dissociation of each Cp ligand can occur from an electric dipole accessible excited electronic state which correlates to the ground electronic state of the photofragments.

We here report the results of a collision-free molecular beam study of both the one and two photon photofragmentation of ferrocene. In these experiments, by measuring the velocity distributions of all the photofragments using a

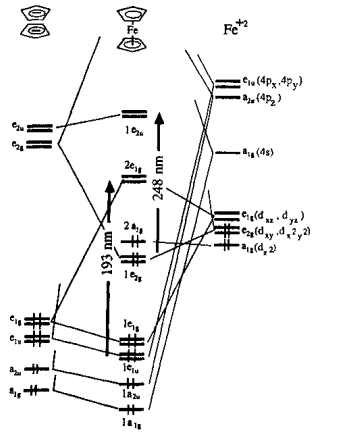

FIG. 2. Molecular orbital diagram for $FeCp_2$ for d^6Fe

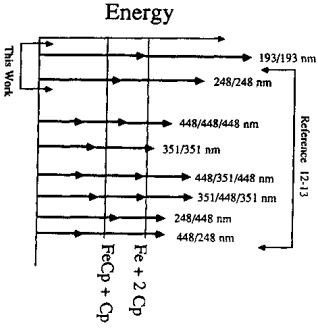

FIG 1 Energetics for the excitations of ferrocene for the present work and that of Liou *et al* in comparison with the bond dissociation energies

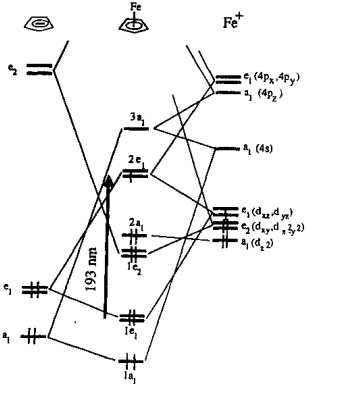

FIG 3 Molecular orbital diagram for FeCp for d^7Fe

crossed laser molecular beam time-of-flight apparatus, we can elucidate many details of the dissociation dynamics for removing both ligands for 193 nm excitation.

EXPERIMENTAL

All of the experimental results were measured using a crossed laser-molecular beam apparatus which detects the neutral photofragments by an electron bombardment ionizer, rf quadrupole mass filter, mass spectrometer. The ionizer is located approximately 21 cm from the intersection point of the collimated laser and molecular beams and the complete mass spectrometer detector assembly can be rotated about the intersection point of the laser and molecular beams. Additional details of the experimental apparatus have been reported in our previous photodissociation study of iron pentacarbonyl.[18] Ferrocene solid (Strem Chemicals) was used without further purification, as the mass spectrum of the molecular beam, shown in Fig. 4, did not show any significant impurity. The molecular beam was formed by flowing argon through the ferrocene container heated to 110 °C (ferrocene vapor pressure 14 Torr[19]) and then expanding the gas mixture through a 0.003 in. diameter stainless steel nozzle maintained at 160 °C using a homebuilt temperature controller. The mass spectrum obtained under these conditions agrees well with the published mass spectral data.[20] In particular, no ion masses heavier than $FeCp_2^+$, which would unambiguously originate from clusters formed in the molecular beam expansion, are detected in the mass spectrum of the molecular beam. The ferrocene velocity distribution was recorded by placing a rotating slotted disk at a known distance from the ionization region as described previously.[18] All photofragment and molecular beam velocity distributions were measured with identical Brink ionizer conditions and 4 mamp emission current. An unfocused excimer laser (Lambda Physik model EMG 103MSC) operating at ArF (193 nm) and KrF (248 nm) with a fluence of 10–30 mJ/cm^2 was used for the photodissociation experiments.

TABLE I. Relative ion signals for 10 000 shots at 193 and 248 nm at a detector angle of 10°.

		ArF		KrF	
Mass	Ion	Signal	Error (2σ)	Signal	Error (2σ)
56	Fe^+	8582	602	587	585
65	Cp^+	707	190	359	206
82	$Fe(C_5H_2)^+$	895	291	...	...
95	$Fe(C_5H_3)^+$	561	278	...	...
121	$FeCp^+$	5304	514	1101	554

The dominant photoproducts are observed at the ions Fe^+, $FeCp^+$, $Fe(C_5H_2)^+$, $Fe(C_5H_3)^+$, and Cp^+. The relative intensities for these ions at a detector angle of 10°, recorded by accumulating 10 000 laser shots for identical laser pulse energies, is given in Table I. Figures 5, 6, and 7 show the measured time-of-flight distributions at the ions Fe^+ (200 000 laser shots), $FeCp^+$ (400 000 laser shots), and Cp^+ (600 000 laser shots) respectively, for the indicated detector angles when ArF laser radiation is used. Figure 6 compares the parent molecular beam velocity distribution measured at $FeCp^+$ with the photofragment velocity distribution of the same ion. Despite the small angular deflection experienced by the photofragments, the comparatively narrow spread of initial ferrocene velocities (speed ratio ~7) allows meaningful extraction of the photofragment velocity distributions, as discussed below. We note from Table I that the photofragment signals are significantly weaker when 248 nm laser radiation is used compared to the signals obtained when 193 nm laser light was used.

For the scattering kinematics of our experiment, the center-of-mass frame velocity distributions can be obtained with semiquantitative accuracy using the *method-of-moments*[21] procedure. The center-of-mass velocity distributions extracted from the experimental data for Fe^+, $FeCp^+$, and Cp^+ at 193 nm are shown in Figs. 8, 9, and 10, respec-

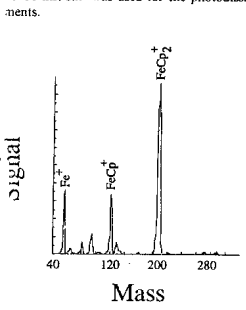

FIG. 4. Mass spectra of the molecular beam. Expansion conditions—3% $FeCp_2$/97% Ar, total pressure 400 Torr, nozzle diameter of 0.003 in, nozzle temperature 160 °C.

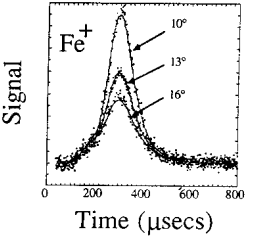

FIG. 5. The measured time-of-flight distribution monitored at Fe^+ for ArF laser radiation at 10° and 13° detector angles. The solid line is the fit to the data using two Gaussians.

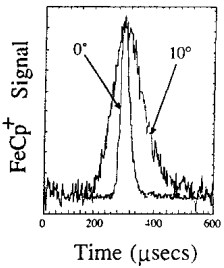

FIG 6. The measured time-of-flight distribution at $FeCp^+$ for ArF laser radiation at 10° with the ferrocene beam velocity distribution measured at $FeCp^+$ with the detector at 0° shown for comparison

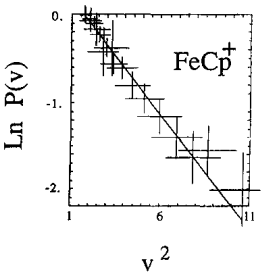

FIG. 9 Extracted center-of-mass velocity distributions using the method of moments for the TOF data taken at $FeCp^+$ for ArF laser radiation with velocities given in units of 10^4 cm/s

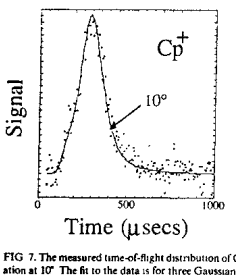

FIG 7. The measured time-of-flight distribution of Cp^+ for ArF laser radiation at 10° The fit to the data is for three Gaussians, where the exponents were fixed to conserve linear momentum for the Gaussians fit at $FeCp^+$ and Fe^+ and to account for FeCp daughter ions

tively. The vertical error bars are 90% confidence interva
computed using the finite number of ion counts assumin
Poisson statistics. For small scattering velocities, the avera
ing caused by the experimental velocity distribution ca
have an important impact on the significance of the TO
measurements. To account for this, the rms scattering ene
gy was computed for each data point. If the difference of t
average energy between two TOF channels was smaller tha
1/4 of the rms energy, then the data from those two chanine
were combined, and a new average and rms energy calcula
ed for the combined data. So long as the difference of averag
scattering energy between the next point and the combine
data point are less than 1/4 of the rms energy, then the ne
point is merged into the combined data. In this fashion, t
many TOF points for slow laboratory velocities which prob
nearly the same scattering velocity can be combined to pr

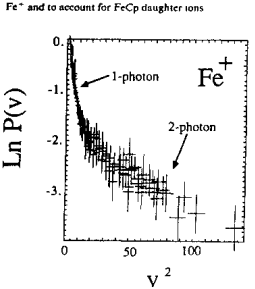

FIG 8 Extracted center-of-mass velocity distributions using the method of moments for the TOF data taken at Fe^+ for ArF laser radiation, with velocities given in units of 10^4 cm/s

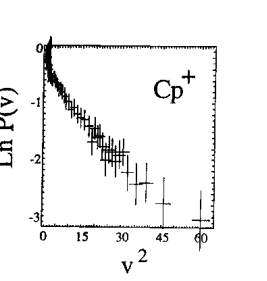

FIG. 10. Extracted center-of-mass velocity distributions using the metho of moments for the TOF data taken at Cp^+ for ArF laser radiation wit velocities given in units of 10^4 cm/s The least squares Gaussian fits are al shown